Chapter 7
Applications of NICE-OHMS to Molecular Spectroscopy

Brian M. Siller and Benjamin J. McCall

Abstract This chapter briefly discusses the general operation of the technique of Noise Immune Cavity Enhanced Optical Heterodyne Molecular Spectroscopy (NICE-OHMS), then goes on to describe the various laser systems that it has been implemented with and the molecules it has been used to study. The relative strengths and weaknesses of each of the laser systems, both in the near- and mid-infrared spectral regions, are highlighted. The molecules that have been studied with NICE-OHMS are described, with particular focus given to those systems that differ in some way from the 'generic' NICE-OHMS setup, and those spectra from which new scientific information was extracted.

7.1 Introduction

Noise Immune Cavity Enhanced Optical Heterodyne Molecular Spectroscopy (NICE-OHMS) is the most sensitive direct absorption technique, as it combines the advantages of cavity enhancement and heterodyne detection for very long effective path lengths through samples and (typically) near shot noise limited detection. Since its first demonstration by Ye et al. [1] in 1998, it has been implemented with a variety of laser systems to study a number of different molecules and extract various information from the obtained spectra.

The technique of NICE-OHMS is discussed thoroughly in another chapter in this book, so only a brief description will be given here. A generic NICE-OHMS experimental setup is shown in Fig. 7.1. The two distinguishing features of NICE-OHMS are an optical cavity and heterodyne detection, with the heterodyne sidebands coupled into separate cavity modes. The optical cavity provides path length enhancement by a factor of $2 \times F/\pi$ compared to a single-pass setup, where F is the cavity

B.M. Siller (✉)
Tiger Optics, 250 Titus Avenue, Warrington, PA 18976, USA
e-mail: bsiller@tigeroptics.com

B.J. McCall
Department of Chemistry, University of Illinois, 600 South Mathews Avenue, Urbana, IL 61801, USA
e-mail: bjmccall@illinois.edu

G. Gagliardi, H.-P. Loock (eds.), *Cavity-Enhanced Spectroscopy and Sensing*, Springer Series in Optical Sciences 179, DOI 10.1007/978-3-642-40003-2_7,

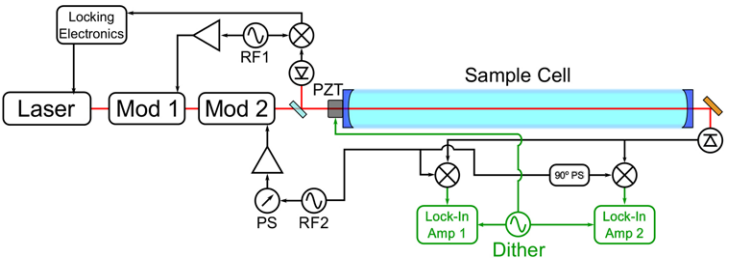

Fig. 7.1 A generic NICE-OHMS experimental layout. The green components are utilized only in wavelength modulated (wm-NICE-OHMS) setups. For fm-NICE-OHMS, the final experimental signals are taken directly from the mixer outputs. Alternatively, in velocity modulation setups, as described in Sects. 7.3.2.2 and 7.3.2.3, the 'dither' is applied to the discharge voltage (not pictured here) across the cell, inducing an alternating Doppler shift of the ions within the cell

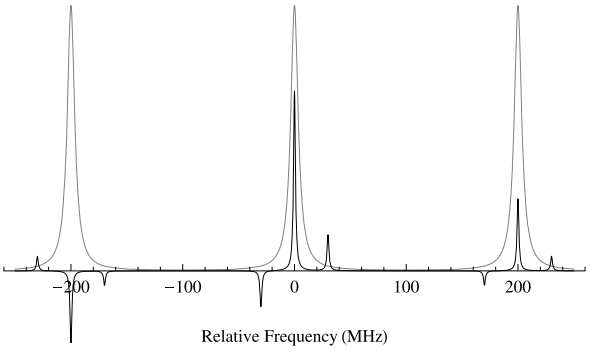

Fig. 7.2 The spectrum of a laser modulated for use in a NICE-OHMS setup overlaid with three optical cavity modes. Note the two sets of sidebands on the laser, in this example spaced at 30 MHz for cavity locking and 200 MHz for heterodyne detection. The second set of sidebands must be spaced at an integer multiple of the cavity FSR. They are most commonly spaced at a single FSR, but can be spaced at two [5] or even nine [6] or more times the free spectral range

finesse, which has ranged from 120 [2] to 100,000 [1] in the various NICE-OHMS implementations.

The laser is modulated at some multiple of the cavity free spectral range (FSR), effectively creating a set of heterodyne sidebands that can be coupled into separate cavity modes, as shown in Fig. 7.2. A second, typically weaker, set of sidebands is added to the laser frequency to enable locking of the laser frequency to the cavity length to constantly keep the carrier frequency on resonance with one of the cavity modes using the Pound-Drever-Hall method [3]. In some NICE-OHMS setups, these two sets of sidebands are also used for locking the sideband spacing to the cavity FSR using the DeVoe-Brewer method [4], to avoid frequency mismatch induced by the cavity FSR changing as its length is scanned.

The frequency modulation is typically applied using a pair of electro-optic modulators (EOM), as in [1], though both sets of sidebands can be applied by a single

EOM if it is capable of simultaneously modulating at two different frequencies with appropriate modulation depths [7]. Or, if the laser frequency can be modulated directly at sufficiently high frequencies, the modulation can be applied to the laser, as in [8].

7.2 Laser Systems

NICE-OHMS has been implemented with a fairly wide variety of laser systems, both in the near- and mid-infrared spectral regions.

7.2.1 Near-Infrared

To date, the vast majority of NICE-OHMS experimental setups have worked in the near-IR spectral region. Near-infrared optical components are generally less expensive, more readily available, and have better performance than the corresponding components designed for the mid-infrared, in part due to the large amount of research and development invested in the field by the telecommunications industry. Component selection is particularly important when it comes to the optical components that need to work at radio frequencies of $\gtrsim$100 MHz, namely a high-speed detector and a method of modulating the laser frequency for heterodyne spectroscopy. Dielectric coatings for cavity mirrors also tend to be better-developed and higher performing in the near-infrared than in the mid-infrared, with losses of up to an order of magnitude lower than the best mid-infrared coatings available.

One disadvantage of working in the near-IR is that no fundamental vibrational bands for molecules lie in this region, so NICE-OHMS spectrometers in this region need to observe overtones or combination bands, which tend to be much weaker than fundamental bands. Since NICE-OHMS is such a sensitive technique, these detections are still possible, but it makes the detection limit in terms of quantity of analyte required for detection significantly larger than it would be for a spectrometer of the same sensitivity observing fundamental band transitions.

7.2.1.1 Neodymium:YAG

NICE-OHMS was first demonstrated by Ye et al. with a Neodymium:YAG (Nd:YAG) laser, and this first demonstration remains to this day the most sensitive NICE-OHMS implementation yet recorded, with a detection sensitivity of 1×10^{-14} cm^{-1} Hz$^{-1/2}$ [1, 9]. One of the scans from this setup is shown in Fig. 7.3, demonstrating the signal-to-noise advantage of NICE-OHMS compared to cavity enhanced absorption spectroscopy (CEAS). This extreme sensitivity was obtained through a combination of very high finesse (100,000) cavity, with a very stable,

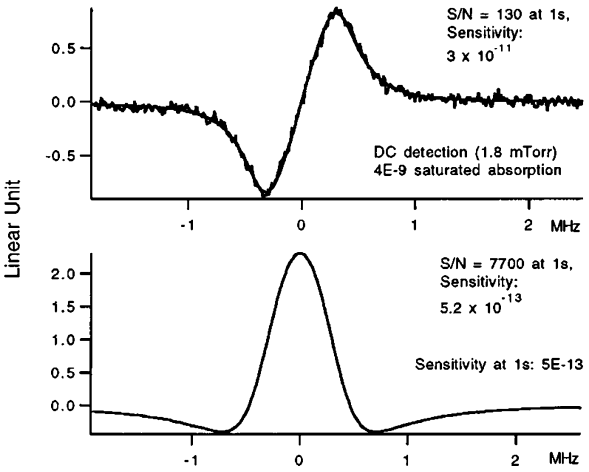

Fig. 7.3 The initial demonstration of NICE-OHMS by Ye et al., from Ref. [1]. Both scans were collected with wavelength-modulated detection of a Lamb dip of acetylene. The top scan is a direct DC detection of the dither signal, while the bottom utilized NICE-OHMS using the same cavity and dither. Fourteen years later, this spectrometer still retains the record for NICE-OHMS detection, with a sensitivity of 5×10^{-13}

well-locked laser (down to 1 mHz relative frequency), and a sensitive detection system that allowed for an observed noise level that was within a factor of 1.4 of the shot noise limit. Although an impressive feat, not much work has been done with Nd:YAG laser systems since, primarily because they are not very widely tunable and thus can't be used to observe a very wide variety of chemical species.

7.2.1.2 Ytterbium:YAG

Ye et al. have also implemented NICE-OHMS with a Ytterbium:YAG (Yb:YAG) laser at 1030 nm [10]. The primary purpose of this work was stabilization of the laser frequency at both short and long timescales, since no precision reference existed at the Yb:YAG wavelength. To that end, a very narrow transition is needed at an absolute frequency. In this work, the R(29) transition of the $3\nu_3$ band of acetylene was used as the absolute frequency reference.

The Yb:YAG beam was sent through a double-pass acousto-optic modulator (AOM), which shifted the frequency of the beam by $\sim$160 MHz without changing the pointing of the beam as the AOM modulation frequency changed. The laser was locked to a stable optical cavity of finesse 75,000 using the Pound-Drever-Hall method. Most of the locking corrections up to 150 kHz control bandwidth were sent to the voltage-controlled oscillator (VCO) that controlled the AOM frequency, while the very slow ($\lesssim$1 Hz) corrections were sent to the Yb:YAG temperature controller. Using these two controls, the absolute laser frequency was stabilized to the cavity to within $\sim$1 kHz relative linewidth, limited primarily by vibrations in the cavity.

For long-term stabilization against drift, a small dither was added to the cavity length, which the laser frequency followed, and a second-harmonic wm-NICE-OHMS signal of the central dispersion Lamb dip was used as an error signal, as its lineshape is antisymmetric. For optimal stabilization, the error signal should have as high a S/N and as narrow a linewidth as possible. In this work, a S/N of 900 was obtained from the sensitivity of 7×10^{-11} at 1 s averaging, and the full width at half

maximum (FWHM) linewidth of the signal was ∼500 kHz, limited by a convolution of transit-time, pressure broadening, and the applied dither. The drift-correction error signal was processed and sent to the piezo-electric transducer on which one of the cavity mirrors was mounted to control the cavity length to prevent the laser frequency from drifting by any more than ∼1 kHz over long timescales.

7.2.1.3 Titanium:Sapphire

Shortly after its initial demonstration with a Nd:YAG, NICE-OHMS was implemented with a Titanium:Sapphire (Ti:Sapph) laser near 790 nm by Ma et al., and its performance was directly compared to that of the Nd:YAG setup [9]. The Ti:Sapph system has the advantage of being much more broadly tunable than the Nd:YAG one, which makes it a much more versatile tool for molecular spectroscopy. Because of this versatility, several other research groups have since implemented Ti:Sapph-based NICE-OHMS spectrometers at wavelengths ranging from 730 nm to 930 nm [6, 11].

The biggest disadvantage of the Ti:Sapph-based system compared to the Nd:YAG one is that the Ti:Sapph has a significantly broader free-running linewidth and cannot be stabilized as tightly to the optical cavity. To extend the bandwidth of the laser-cavity lock, double-pass AOMs have been used to provide a higher-frequency transducer to the system [6, 9]. To extend the bandwidth even further, a third EOM can be used with a sweeping applied voltage to change the laser frequency even faster than the AOM allows, since the EOM is not limited by the propagation time of an acoustic wave through a crystal, as an AOM is [9]. With both of these extra frequency transducers, Ma et al. were able to stabilize the Ti:Sapph laser to a cavity of finesse 17,000 to within a relative linewidth of 400 mHz. This is more than satisfactory for performing NICE-OHMS, but is still a factor of ∼300 lower in sensitivity than they were able to achieve with the Nd:YAG setup and cavity with 100,000 finesse.

7.2.1.4 External Cavity Diode Lasers

NICE-OHMS has also been implemented with different types of diode lasers, including external-cavity diode lasers (ECDL) and distributed feedback (DFB) diode lasers. Both of these types of diode lasers have the advantages of being relatively inexpensive and much more broadly tunable than the relatively fixed-frequency YAG-based lasers.

For example, Bell et al. built an ECDL-based NICE-OHMS spectrometer for studying the HO_2 radical (see Sect. 7.3.2.1), and also used it to study CH_4 and CO_2 as diagnostic tests of their system [5]. In working with their system, they found that the sensitivity varied significantly with wavelength; they attributed this to the response of the laser varying as the wavelength was tuned, particularly with respect to the locking corrections being sent to the laser current. At 6596 cm^{-1}, where they optimized the system, they could achieve a sensitivity of 3×10^{-11} cm^{-1} with wm-

NICE-OHMS, but tuning the laser by ∼40 cm^{-1} to the red limited their sensitivity to 2×10^{-10} cm^{-1}. This is still very sensitive in absolute terms, but is nearly an order of magnitude less sensitive than their optimal value; this shows that optimizing a NICE-OHMS system under a particular set of conditions does not necessarily optimize it over a broad range of conditions.

Gianfrani et al. used a similar ECDL-based setup to study molecular oxygen (see Sect. 7.3.1.5) [12]. One unique aspect of their setup was the way in which they locked the heterodyne frequency to the cavity FSR. Rather than using the common DeVoe-Brewer method, they applied a small dither to the RF frequency at 70 kHz, demodulated the cavity back-reflection signal at that frequency, and used the resulting signal as an error signal for locking the sideband spacing to exactly the cavity FSR with a locking bandwidth of ∼10 kHz. They also found that the locking corrections being sent to the laser injection current produced significant intensity noise, so to combat this effect, they used an AOM in another feedback loop to keep the laser power as constant as possible. They did this because while in principle, the noise-immune property of NICE-OHMS prevents laser intensity noise from contributing to the net spectroscopic signal, in practice, residual amplitude modulation (RAM) is always present, and can cause laser intensity noise to couple through the entire detection train and into the final signal. This effect of RAM often makes it worth taking the time to clean up whatever intensity noise there is, rather than relying on the noise-immune property to maximize the sensitivity of the instrument. The intensity stabilizer not only improved their sensitivity, but also allowed them to collect broad scans (up to 8 GHz wide) with very flat baselines.

7.2.1.5 Distributed Feedback Diode Lasers

NICE-OHMS has also been implemented with a distributed feedback (DFB) diode laser [13]. Compared to ECDLs, DFB lasers are more robust, since they don't rely on an external grating that is susceptible to mechanical vibrations, so they have greater potential for use in more robust spectrometers. The DFB laser used in this work has the additional advantage of having a fiber-coupled output, which makes it easier to use the fiber-coupled acousto-optic and electro-optic modulators that were used for modulation and locking. Compared to free-space components, fiber components tend to be significantly easier to align and use, and often have better performance than their free-space counterparts.

7.2.1.6 Fiber Lasers

Fiber lasers offer excellent frequency stability and mode structure, which makes them well-suited for efficient coupling into and locking to optical cavities. Since the laser is fiber-coupled to start with, and exits the fiber in free space before entering the optical cavity, the instrument designer has a choice of using either fiber or free-space components for laser frequency modulation and control. Fiber EOMs are particular attractive for NICE-OHMS since they are much more efficient (lower

half-wave voltage) compared to free space EOMs without the need for a resonant electronic circuit to amplify effective RF voltages. This allows for the laser frequency to be modulated at essentially any frequency up to several GHz with almost arbitrary depth of modulation. It is also possible to apply both of the modulation signals needed (for locking and for heterodyne detection) to a single EOM by using a simple RF combiner. Schmidt et al. demonstrated NICE-OHMS with an erbium-doped fiber laser, and observed acetylene with a sensitivity of 2.4×10^{-9} cm^{-1}, which was about a factor of 1000 above the shot noise limit [7]. In a follow-up paper in which they used a different EOM with shorter fibers and used an active temperature controller for the temperature of the EOM and fibers, they improved the sensitivity to 5×10^{-11} cm^{-1} Hz$^{-1/2}$, which is within a factor of 26 of the shot noise limit [14].

7.2.2 Mid-Infrared

NICE-OHMS hasn't been implemented nearly as often in the mid-infrared as it has in the near-infrared, in part because high performance mid-infrared components are not very readily available, but the mid-infrared does offer the significant advantage of being the region of fundamental vibrational modes of many molecules. In the decade following the initial discovery of NICE-OHMS, only a single demonstration was done at wavelengths beyond 2 μm, which used a quantum cascade laser (QCL) at ~8.5 μm. Recently, mid-infrared systems have been implemented using nonlinear processes to frequency-shift near-IR lasers into the mid-IR. This allows for all laser processing to be done on the near-IR systems, meaning the only specialized mid-IR components required are cavity mirrors with appropriate coatings and fast detectors.

7.2.2.1 Quantum Cascade Lasers

Quantum cascade lasers (QCL) offer the advantage of being available at wavelengths ranging from 3.5 to 20 μm, a range inaccessible by most laser systems. Taubman et al. demonstrated a QCL-based NICE-OHMS spectrometer at ~8.5 μm with a sensitivity of 9.7×10^{-11} cm^{-1} Hz$^{-1/2}$ [8]. They had two major difficulties in setting up this system: modulating the QCL, and detecting the resulting heterodyne beat signal, both of which typically need to operate with bandwidths of hundreds of MHz.

Frequency modulating the QCL was accomplished by modulating its injection current. They found that the modulation efficiency fell proportional to $1/f$, where f is the modulation frequency, up to ~100 MHz, and dropped proportional to $1/f^2$ above 100 MHz. They did, however find a resonance in their QCL at 387.5 MHz where the modulation efficiency was significantly higher than nearby frequencies, so they chose this as their heterodyne frequency and designed their optical cavity length to match. They didn't offer a physical explanation for the resonance, but they note that resonant frequencies vary between different lasers, even for lasers on

the same chip. This paper also describes a scheme for modulating a QCL with an injection-locking scheme using two lasers, a master and a slave, and they showed that this method reduced the observed RAM level by 49 dB compared to the current modulation scheme that was used for spectroscopy. Although this modulation scheme has not yet been used in a NICE-OHMS system, it is promising for future work.

The other challenge they faced was finding and characterizing a detector fast enough for optimal heterodyne detection. They used a mercury-cadmium-telluride (MCT) detector, and to determine its frequency response, they used two separate QCLs, tuned them to slightly different frequencies, and combined them onto the detector element. This gave them a heterodyne beat that should have constant amplitude over the ~800 MHz that they tuned the frequency difference. By recording the detector output signal versus the heterodyne frequency, they found that the net detector signal at 387 MHz was attenuated by 35 dB compared to the DC response, and they attribute this detector inefficiency as the reason for their detection sensitivity being an order of magnitude above the shot noise limit.

One of the limitations of working with QCL systems is the limited tunability, which can be anywhere from ~20 cm^{-1} (for stand-alone QCL systems such as the one used for NICE-OHMS) to ~200 cm^{-1} (for external-cavity systems).

7.2.2.2 Difference Frequency Generation

Recently, NICE-OHMS has been implemented with a broadly tunable mid-IR source through difference frequency generation (DFG) [15]. The DFG process works by combining two lasers within a nonlinear material to produce a beam whose frequency is the difference of the two input lasers' frequencies. This experimental setup was based around a fixed-frequency Nd:YAG laser and a tunable Ti:Sapph laser, which were combined in a periodically poled lithium niobate (PPLN) crystal. Because near-IR components typically have better performance, lower prices, and are more readily available than their mid-IR counterparts, all laser frequency control was done on the near-IR pump lasers before generating the mid-IR DFG, so the only mid-IR specific components that were needed were the detectors for cavity transmission and back-reflection, and the cavity mirrors, which were specified for the 3.0–3.4 μm range. The 2.8–4.8 μm tuning range of the laser system, limited by the poling periods of the PPLN crystal, is a particularly attractive range for fundamental vibrational modes of many molecules.

To minimize the effects of frequency-dependent RAM and etalon effects on the ultimate signal from the instrument, the two EOMs were both placed on the fixed-frequency Nd:YAG rather than the tunable Ti:Sapph. The system remains sensitive to any etalons on the mid-IR beam after the PPLN crystal, but it is insensitive to those effects on either of the two near-IR beams.

This DFG system was used to acquire spectra of methane with both fm- and wm-NICE-OHMS. The fm-NICE-OHMS setup was used to acquire Doppler-broadened scans, and its sensitivity of 2×10^{-7} cm^{-1} $Hz^{-1/2}$ was limited primarily by etalons

in the mid-IR beam path, particularly between the PPLN crystal and the cavity input mirror and between the cavity output mirror and the detector. In the wm-NICE-OHMS setup, a 50 Hz dither was added with a 1.7 MHz peak-to-peak modulation to observe just the sub-Doppler features of methane. In this configuration, the sensitivity was over an order of magnitude better: 6×10^{-9} cm^{-1} Hz$^{-1/2}$, approximately a factor of 60 above the shot noise limit.

7.2.2.3 Optical Parametric Oscillators

Recently, NICE-OHMS has also been implemented with an optical parametric oscillator (OPO), which relies on a nonlinear process similar to that used in the DFG system [2]. A 1064 nm ytterbium-doped fiber laser was used as the seed. This beam was passed through a fiber EOM that applies both the locking and heterodyne sidebands before the beam is sent to a fiber amplifier, which amplifies the total laser power to ∼10 W to be used as the pump of the OPO.

The OPO consists of a fan PPLN, which enables continuous tuning of the poling periods across its range by translating the crystal, and a singly resonant cavity, that is resonant with just the signal beam of the OPO. The signal is tunable from 1.5–1.6 μm, while the idler is tunable from 3.2–3.9 μm. Because the locking and heterodyne sidebands on the pump beam are not spaced at an exact multiple of the FSR of the OPO signal cavity, the signal beam remains a single frequency. Due to conservation of energy, this means that the sidebands get transferred entirely to the idler beam.

The NICE-OHMS cavity used in this work had a fairly low finesse, ∼120, but with the idler power of ∼1 W, there was more than enough intracavity power to enable sub-Doppler spectroscopy of molecular ions. Velocity modulation was coupled with NICE-OHMS in a technique referred to as Noise Immune Cavity Enhanced Optical Heterodyne Velocity Modulation Spectroscopy (NICE-OHVMS). Not only does velocity modulation help to combat some of the difficulties associated with DC detection (e.g. RAM and etalons), but it also affords discrimination of ionic signals from neutral ones through phase sensitive detection. After RF demodulation to separate absorption from dispersion followed by a second level of demodulation at twice the plasma drive frequency, a total of four data channels were collected simultaneously. There was some significant fringing in the signals from three of the detection channels, and the quietest of the channels exhibited a sensitivity of 3.9×10^{-9} cm^{-1}.

7.3 Molecules

Several different molecules have been observed with the NICE-OHMS spectrometers described Sect. 7.2. Many of these have been chosen to demonstrate and optimize spectrometers because they have bands that coincide with the spectral coverage of the laser systems used, while others were observed based on scientific

interest and NICE-OHMS was the technique of choice due to its sensitivity and resolution. This section is intended to give an overview of the molecules observed with NICE-OHMS to date, briefly mentioning the molecules that were used as tests to demonstrate the capabilities of instruments, while discussing more in depth the studies from which new molecular information was extracted from NICE-OHMS spectra.

7.3.1 Stable Neutral Molecules

The vast majority of NICE-OHMS papers that have been published to date have demonstrated the detection of stable neutral molecules. Typically, these spectrometers have a static sample cell, often made of Invar, Zerodur, or some other material with a low coefficient of thermal expansion, with the cavity mirrors permanently affixed to the cell, and one mirror mounted on a piezo-electric transducer.

7.3.1.1 Acetylene (C_2H_2)

For many of the papers whose primary purpose was to demonstrate the technique of NICE-OHMS and to characterize and optimize the various aspects of the technique, acetylene and its isotopologues have been favorite targets [1, 7, 16–18]. Several vibrational combination bands have been observed at wavelengths ranging from 730 nm to 1530 nm.

7.3.1.2 Methane (CH_4)

Bell et al. observed an unassigned methane transition at 6610.06 cm^{-1} as a diagnostic of their NICE-OHMS spectrometer described in Sect. 7.3.2.1, recording the pressure broadening in helium to verify the linearity of their spectrometer [5]. Their pressure-broadening coefficient of 1.5 ± 0.1 MHz/Torr (HWHM) agreed well with the literature values for the $2\nu_3$ band of methane at 1.65 μm.

Ishibashi et al. observed several lines of the $2\nu_3$ band of methane with their ECDL-based wm-NICE-OHMS spectrometer with sub-Doppler resolution [19]. They also observed several lines of $^{13}CH_4$, and used their acquired spectra to determine that their sensitivity was 9.5×10^{-11} cm^{-1}, which is within a factor of 2.6 of the shot noise limit, and that their spectral resolution was 320 kHz, limited primarily by transit time, but with a small contribution from residual frequency noise in the system.

Porambo et al. used methane to demonstrate the capabilities of their DFG-based NICE-OHMS spectrometer [15]. They performed both Doppler-broadened scans with fm-NICE-OHMS, and sub-Doppler scans with wm-NICE-OHMS. They observed several transitions of the ν_3 fundamental band of CH_4, and found that they could obtain a sensitivity of $\sim 6 \times 10^{-9}$ cm^{-1} $Hz^{-1/2}$.

7.3.1.3 Methyl Iodide (CH_3I)

Ishibashi et al. also used their ECDL-based NICE-OHMS setup to observe the $2\nu_4$ band of CH_3I centered around 1.65 μm [20]. They observed a total of 56 rovibrational transitions from the P, Q, and R branches with ∼1 MHz resolution. This allowed them to achieve full resolution of the electric quadrupole hyperfine components for the P and R branch lines, while the Q branch hyperfine components were partially blended. Because the hyperfine splitting pattern differs for different spectral lines, they found that hyperfine resolution was useful for assigning their acquired spectra.

7.3.1.4 Nitric Oxide (NO)

Bood et al. studied the sixth overtone band of nitric oxide near 797 nm in order to determine its transition dipole moment [17]. This high overtone band is too weak for most direct absorption techniques, which is why NICE-OHMS was chosen. They observed a total of 15 rovibrational transitions of the ${}^2\Pi_{1/2}$–${}^2\Pi_{1/2}$ sub-band of this vibrational band at a pressure of 75 Torr, and from their data, they extracted absolute intensities of individual lines, the vibrational transition dipole moment, and Herman-Wallis coefficients. Comparing the transition dipole moment of 3.09 μD for this band to the lower overtone bands indicated a significant influence from anharmonicity at the $v = 7$ vibrational level. They also parametrized the electric dipole moment of NO for bond lengths ranging between 0.91 and 1.74 Å more accurately than had previously been done.

7.3.1.5 Molecular Oxygen (O_2)

Gianfrani et al. used an ECDL and a cavity of finesse 6,000 to perform NICE-OHMS of molecular oxygen with a sensitivity of 6.9×10^{-11} $cm^{-1}\,Hz^{-1/2}$, a factor of 30 above the shot noise limit [12]. They studied weak magnetic-dipole transitions of the $b^1\Sigma_g^+(v' = 0) \leftarrow X^3\Sigma_g^-(v'' = 0)$ band near 762 nm. They started by characterizing their spectrometer in both fm- and wm-NICE-OHMS modes of operation using the ${}^PQ(13)$ line of ${}^{16}O_2$ with 50 mTorr of pressure, looking at both lineshapes and sensitivity compared to direct CEAS detection.

They then went on to look for the ${}^{16}O_2$ ${}^PP(12)$ forbidden transition. As a consequence of the symmetrization postulate of quantum mechanics, transitions starting from even rotational quantum numbers are forbidden, so they used their NICE-OHMS spectrometer to look for one of these forbidden transitions as a test of this postulate. They saw no trace of a signal at up to 200 Torr of pressure, so based on their calculated sensitivity, they could set the upper limit on the violation of the symmetrization postulate for O_2 at 5×10^{-8}, which is about an order of magnitude lower than the previous upper limit.

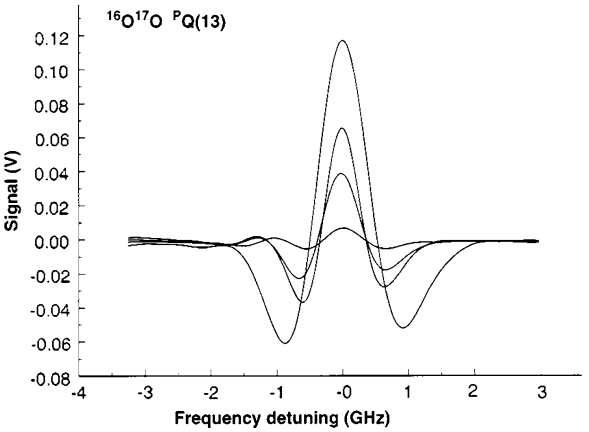

Fig. 7.4 NICE-OHMS signal from Gianfrani et al. [12] of the ^{P}Q(13) line of $^{16}O^{17}O$ in its natural abundance (0.037 %) at 764.489 nm for four different pressures ranging from 660 to 1.3×10^4 Pa

As shown in Fig. 7.4, they also observed some weak lines of $^{16}O^{18}O$ and $^{16}O^{17}O$ in their natural abundances (0.2 % and 0.037 %, respectively), and noted some nonlinearity with pressure that they attributed to two factors: the onset of pressure broadening at higher pressures, and the decreasing modulation depth of their constant-amplitude dither as linewidths broadened at higher pressures.

7.3.1.6 Nitrous Oxide (N_2O)

Taubman et al. characterized their QCL-based NICE-OHMS spectrometer with a nitrous oxide line at 1174.9515 cm^{-1} [8]. They used the observed spectra to determine that their experimental sensitivity was 9.72×10^{-11} $cm^{-1}\,Hz^{-1/2}$, and compared the obtained NICE-OHMS signals to those obtained with CEAS, showing the drastic noise reduction enabled by the technique.

Bell et al. performed spectroscopy of the R28(e) transition of the ν_3 band of N_2O as another diagnostic of their spectrometer described in Sect. 7.3.2.1 [5]. They found the pressure-broadening coefficient of 2.2 ± 0.1 MHz to be in good agreement with the literature value of the P(26) transition of the same band, and furthermore verified the linearity of their detection system, as indicated by the linear fit of the linewidth versus pressure plot.

7.3.1.7 Carbon Dioxide (CO_2)

Bell et al. also performed spectroscopy on the $\nu_1 + \nu_2 + 2\nu_3$ band of carbon dioxide at 6646.58 cm^{-1} as a diagnostic test of their ECDL-based NICE-OHMS spectrometer whose primary purpose was spectroscopy of HO_2 radical (see Sect. 7.3.2.1). They achieved a sensitivity of 2×10^{-10} cm^{-1} in 10 s of averaging, which was two orders of magnitude more sensitive than their CEAS setup with the same cavity.

7.3.2 Radicals and Ions

More recently, NICE-OHMS has been used to observe HO_2, N_2^+, and H_3^+. The sensitivity of NICE-OHMS is very well suited to detection of these species, since under the conditions used to generate these species, radicals and ions are often orders of magnitude less abundant than their precursor molecules.

7.3.2.1 Hydroperoxyl Radical (HO_2)

The HO_2 radical, which is of interest to atmospheric chemistry, has recently been studied using NICE-OHMS by Bell et al. [5] NICE-OHMS was chosen as the optimal technique due to its species-specific detection (as opposed to some other indirect techniques that have been used for this molecule), its capability of extracting absolute number densities from spectra, and its extremely high sensitivity. The first vibrational overtone of the OH stretch ($2\nu_1$) band, centered at 6649 cm^{-1}, was studied in this work, as it falls within the range of the ECDL used (1480–1540 nm).

Both fm- and wm-NICE-OHMS were performed. Heterodyne sidebands were spaced at ~219 MHz, twice the cavity's FSR, and this frequency was locked using the DeVoe-Brewer method. For the wavelength-modulated work, a 60 Hz dither was applied to one of the cavity mirrors to induce a frequency dither with 100 MHz amplitude. By performing cavity-enhanced absorption spectroscopy (CEAS) of a known transition of methane at 6595.90 cm^{-1} within their spectrometer, the authors determined that their cavity finesse was 2100 ± 100.

Within the vacuum chamber, 2 cm above the cavity, five UV lamps were used for photolysis of Cl_2. The generated Cl atoms then reacted with methanol to form CH_2OH, which then reacted with O_2 to form HO_2 and formaldehyde. The authors performed a detailed chemical analysis of all reactions to take place within the chamber to predict the abundance of HO_2 as well as that of any potentially interfering species.

Two transitions of the first vibrational overtone of the OH stretch ($2\nu_1$) were studied: the $^qP_1(12)$ transition at 6623.32 cm^{-1}, and the $^qP_2(10)$ transition at 6623.57 cm^{-1}, as shown in Fig. 7.5. fm-NICE-OHMS was performed, and background scans were collected and subtracted by turning off the UV lamps for ~10 s and repeating the scans. A sensitivity of 1.8×10^{-9} cm^{-1} was achieved, which corresponded to a minimum detectable concentration of $\sim 4 \times 10^{10}$ radicals/cm^3.

Kinetic studies were performed by turning off either the chlorine gas flow or the UV lamps, and observing the rate at which the observed signal decayed. The observed signal loss rate combined with kinetic modeling provided further evidence that the observed lines were, in fact, from the HO_2 radical and not some other species in the sample cell. The authors also used the decay rate to estimate the rate at which HO_2 is broken down by the walls of the chamber.

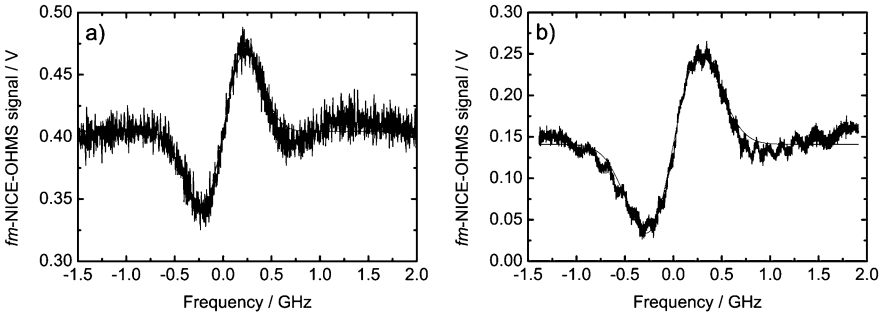

Fig. 7.5 fm-NICE-OHMS spectra of HO_2 with fits from Bell et al. [5] (**a**) $^qP_1(12)$ transition at 6623.32 cm^{-1}, (**b**) $^qP_2(10)$ transition at 6623.57 cm^{-1}

7.3.2.2 Molecular Nitrogen Cation (N_2^+)

N_2^+ has recently been studied with NICE-OHMS in both positive column [6] and ion beam [21] experiments. Both of these experiments relied on the same Ti:Sapph laser system, and because the cavity mirrors were physically separated from the sample cells, the positive column cell and the ion beam chamber could be moved in and out of the cavity without the need for a full optical realignment.

The cavity in both experiments had a finesse of ~300 and a free spectral range of ~113 MHz, and both experiments observed several transitions in the $\nu = 1 \leftarrow 0$ band of the Meinel system ($A^2\Pi_u$–$X^2\Sigma_u^+$) of N_2^+. Both also used a form of velocity modulation in addition to the usual NICE-OHMS heterodyne modulation.

In the positive column work, a plasma discharge cell was placed within the cavity, and light was coupled through Brewster windows mounted on either side of the cell. Two different heterodyne configurations were used: one with sidebands spaced at 1.02 GHz, 9 times the cavity free spectral range, and the other with sidebands spaced at 113 MHz, a single cavity free spectral range. A sample 9FSR scan is shown in Fig. 7.6.

The plasma discharge voltage was modulated at 40 kHz, and the net signal was demodulated at twice that frequency to extract both the velocity- and concentration-modulated components of the ion signals, as well as the concentration-modulated signals of any excited neutral species. The 9-FSR setup was used to collect wide Doppler broadened scans of N_2^+ and N_2^* (an electronically excited state of neutral N_2), while the 1-FSR setup was used to primarily to collect scans of the sub-Doppler features at the center of the N_2^+ lineshapes. The Lamb dips were found to have much steeper pressure broadening (~8 MHz/Torr) than that of typical neutral molecules, as well as an extrapolated zero-pressure linewidth of ~32 MHz, which isn't fully understood at this point.

Sub-Doppler scans were calibrated with an optical frequency comb, and with the extreme absolute accuracy afforded by comb calibration and the precision afforded by sub-Doppler resolution, line centers were determined with an absolute accuracy of ~300 kHz, which is approximately two orders of magnitude more pre-

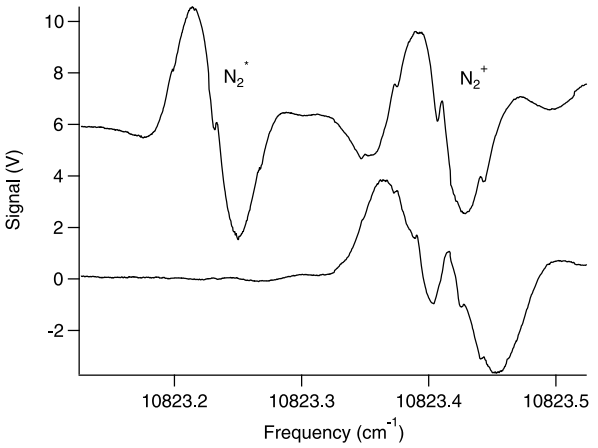

Fig. 7.6 A signal from the NICE-OHVMS system with a nitrogen plasma. The two traces are from the X and Y outputs of the lock-in amplifier. For this scan, the heterodyne sidebands were spaced at ∼1 GHz, so Lamb dips are spaced at ∼500 MHz on top of the Doppler profiles. Two spectral lines are shown, one from N_2^+ that is both concentration- and velocity-modulated, and the other from N_2^* that is just concentration-modulated. The RF detection phase was tuned to show primarily the dispersion signal, as evidenced by the strong central Lamb dips, and the plasma detection phase was tuned to isolate all of the N_2^* in a single detection phase

cise than traditional Doppler-broadened, wavemeter-calibrated velocity modulation spectroscopy.

For the ion beam work, the plasma discharge cell was removed from the optical cavity, and was replaced by a large vacuum chamber containing the ion beam and its associated ion optics. To avoid vibrations from the turbo pumps coupling into the cavity mirrors (and thus making locking more difficult), the ion beam chamber was mechanically separated from the optical setup, resting directly on the lab floor while all of the optics, including the cavity mirrors, were mounted on a floated optics table. Again, light was coupled through Brewster windows that were mounted on the sides of the chamber, and the ion beam within the chamber was made collinear with the intracavity laser beam by moving the chamber (for coarse control) and steering the ion beam by tuning voltages on the various ion optics (for fine control).

The ions were extracted from the source and accelerated through a 3.8 kV potential drop before being steered through a metal tube along the collinearity path of the ion and laser beams. Velocity modulation was accomplished by applying a 4 kHz 2 V peak-to-peak square wave voltage to the metal drift tube. The NICE-OHMS signal was then demodulated at this modulation frequency to extract the ion signal. Because the modulation voltage required in this setup was quite small, very little electrical interference was introduced by it, as opposed to the positive column cell that used kV-level modulation voltages. Also, the modulation is completely independent of the laser, unlike wm-NICE-OHMS, which can still be somewhat sensitive to RAM and etalons. This allowed this spectrometer to obtain a noise-equivalent

absorption of $\sim 2 \times 10^{-11}$ cm^{-1} Hz$^{-1/2}$, within a factor of 1.5 of the shot noise limit.

The lines observed by this instrument are Doppler-shifted by ~ 6 cm^{-1} from their rest frequencies, and the linewidths obtained are narrowed through kinematic compression to ~ 120 MHz, which was limited by the beam energy spread of the ions extracted from the source into the beam. With frequency comb calibration, transition rest frequencies were determined to within ~ 8 MHz of those determined by the NICE-OHVMS work [6], which measured transition rest frequencies directly. The accuracy was limited by the asymmetry observed in the lineshapes, which is thought to be caused by imperfect alignment of the two beams and the beam energy stability over time.

7.3.2.3 Trihydrogen Cation (H_3^+)

The technique of NICE-OHVMS, which combines NICE-OHMS with velocity modulation spectroscopy within a positive column discharge cell, has been extended into the mid-infrared using an OPO, as described in Sect. 7.2.2.3, and its capabilities were demonstrated by observing H_3^+ in a liquid nitrogen cooled discharge cell, which lowered the rotational temperature of the ions to ~ 300 K, compared to the 600–700 K temperatures that are typical for air-cooled cells [2].

Like the N_2^+ work, the detector signal was demodulated twice, first at the heterodyne frequency with two RF mixers, then at twice the plasma frequency using a pair of dual-channel lock-in amplifiers. Since the technique of NICE-OHVMS is sensitive to both concentration- and velocity-modulated signals, all four detection channels had some signal, and these signals were not completely separable from one another. This makes fitting the Doppler profiles of the acquired signals difficult, so it was not attempted in this work.

Because Lamb dips probe only the zero-velocity population, velocity modulation of the overall ion population does not have the same effect on the signal as it does for the Doppler profile. Rather, the zero-velocity population increases and decreases throughout the cycles of the plasma discharge, so both velocity- and concentration-modulated signals appear as concentration modulation when just the zero-velocity population of the ions is considered.

Both the $R(1,0)$ and $R(1,1)^u$ lines of H_3^+, which are separated by ~ 0.3 cm^{-1}, were collected in a continuous scan. The overall continuous tuning range of this system is ~ 8 cm^{-1}, limited by the tuning range of the fiber seed laser, and the overall wavelength coverage of the OPO system is 3.2–3.9 μm, though with additional OPO modules, the tuning range could be extended to 2.2–4.6 μm, limited by the transparency of lithium niobate.

Finer resolution scans were collected of just the $R(1,0)$ line, and the four data channels acquired from each scan were fit simultaneously to find a linecenter. Although the accuracy of linecenter determination was limited to ~ 100 MHz by the wavemeter calibration, the precision of the fit was found to be ~ 70 kHz, which represents the ultimate limit that could be obtained if one were to calibrate the spectra

with a more accurate method, e.g. with an optical frequency comb. The Lamb dips were found to each be ~110 MHz wide (FWHM), so each individual Lamb dip was not resolvable, since the Lamb dips are spaced by FSR/2, ~40 MHz.

7.4 Future Prospects

Even though NICE-OHMS has been implemented by a number of research groups over the past 15 years, we have still only begun to scratch the surface of what NICE-OHMS makes possible. The recent developments extending NICE-OHMS into the mid-infrared hold promise to enable the detection of strong fundamental bands of a greater variety of molecules. There has also been a good deal of work attempting to make NICE-OHMS a more robust technique, one that has the potential in being deployed in more robust instruments to observe trace gases in a wider variety of environments rather than being confined to a laboratory setting.

References

1. J. Ye, L.S. Ma, J.L. Hall, J. Opt. Soc. Am. B **15**(1), 6 (1998). doi:10.1364/JOSAB.15.000006. http://josab.osa.org/abstract.cfm?URI=josab-15-1-6
2. K.N. Crabtree, J.N. Hodges, B.M. Siller, A.J. Perry, J.E. Kelly, P.A. Jenkins, B.J. McCall, Chem. Phys. Lett. (2012). doi:10.1016/j.cplett.2012.09.015. http://www.sciencedirect.com/science/article/pii/S0009261412010597
3. R.W.P. Drever, J.L. Hall, F.V. Kowalski, J. Hough, G.M. Ford, A.J. Munley, H. Ward, Appl. Phys. B, Lasers Opt. **31**, 97 (1983). doi:10.1007/BF00702605. http://dx.doi.org/10.1007/BF00702605
4. R.G. DeVoe, R.G. Brewer, Phys. Rev. A **30**, 2827 (1984). doi:10.1103/PhysRevA.30.2827. http://link.aps.org/doi/10.1103/PhysRevA.30.2827
5. C.L. Bell, J.P.H. van Helden, T.P.J. Blaikie, G. Hancock, N.J. van Leeuwen, R. Peverall, G.A.D. Ritchie, J. Phys. Chem. A **116**(21), 5090 (2012). doi:10.1021/jp301038r
6. B.M. Siller, M.W. Porambo, A.A. Mills, B.J. McCall, Opt. Express **19**(24), 24822 (2011)
7. F.M. Schmidt, A. Foltynowicz, W. Ma, O. Axner, J. Opt. Soc. Am. B **24**(6), 1392 (2007). doi:10.1364/JOSAB.24.001392
8. M.S. Taubman, T.L. Myers, B.D. Cannon, R.M. Williams, Spectrochim. Acta, Part A, Mol. Biomol. Spectrosc. **60**(14), 3457 (2004). doi:10.1016/j.saa.2003.12.057. http://www.sciencedirect.com/science/article/pii/S1386142504001258
9. L. Ma, J. Ye, P. Dube, J. Hall, J. Opt. Soc. Am. B **16**(12), 2255 (1999). doi:10.1364/JOSAB.16.002255
10. J. Ye, L.S. Ma, J.L. Hall, J. Opt. Soc. Am. B **17**(6), 927 (2000). doi:10.1364/JOSAB.17.000927. http://josab.osa.org/abstract.cfm?URI=josab-17-6-927
11. A. Foltynowicz, F.M. Schmidt, W. Ma, O. Axner, Appl. Phys. B, Lasers Opt. **92**(3), 313 (2008). doi:10.1007/s00340-008-3126-z
12. L. Gianfrani, R.W. Fox, L. Hollberg, J. Opt. Soc. Am. B **16**(12), 2247 (1999). doi:10.1364/JOSAB.16.002247. http://josab.osa.org/abstract.cfm?URI=josab-16-12-2247
13. A. Foltynowicz, J. Wang, P. Ehlers, O. Axner, Opt. Express **18**(18), 18580 (2010)
14. A. Foltynowicz, W. Ma, O. Axner, Opt. Express **16**(19), 14689 (2008). http://www.opticsexpress.org/viewmedia.cfm?uri=oe-16-19-14689

15. M.W. Porambo, B.M. Siller, J.M. Pearson, B. McCall, Opt. Lett. **37**, 4422 (2012). doi:10.1364/OL.37.004422
16. F.M. Schmidt, A. Foltynowicz, W. Ma, T. Lock, O. Axner, Opt. Express **15**(17), 10822 (2007). doi:10.1364/OE.15.010822
17. J. Bood, A. McIlroy, D.L. Osborn, J. Chem. Phys. **124**(8), 084311 (2006). doi:10.1063/1.2170090. http://link.aip.org/link/?JCP/124/084311/1
18. W. Ma, A. Foltynowicz, O. Axner, J. Opt. Soc. Am. B **25**(7), 1144 (2008). doi:10.1364/JOSAB.25.001144
19. C. Ishibashi, H. Sasada, Jpn. J. Appl. Phys. **38**(Part 1, No. 2A), 920 (1999). doi:10.1143/JJAP.38.920. http://jjap.jsap.jp/link?JJAP/38/920/
20. C. Ishibashi, H. Sasada, J. Mol. Spectrosc. **200**(1), 147 (2000)
21. A.A. Mills, B.M. Siller, M.W. Porambo, M. Perera, H. Kreckel, B.J. McCall, J. Chem. Phys. **135**(22), 224201 (2011). doi:10.1063/1.3665925